Feasible Study of Spray and Combustion Control Using Dual Component Fuel Based on Multicomponent Spray Model

Y. Kobashi* and J. Senda**
*Department of Mechanical Engineering, Kanazawa Institute of Technology
7-1 Ohgigaoka, Nonoichi, Ishikawa, 921-8501 Japan
**Department of Mechanical Engineering, Doshisha University

Abstract

To achieve further improvement of thermal efficiency and exhaust emissions in compression ignition engines, the authors propose a control technique of spatial-temporal spray and combustion processes by use of dual component fuels. In order to ensure the feasibility of this approach, the present study evaluates spray characteristics of dual component fuels and examines the feasibility of this proposal by use of a multicomponent spray model which had been developed by the authors and incorporated into KIVA-3V. Four dual component fuels exhibiting a range of volatility were used to evaluate the accuracy of this model and to understand the effects of vapor-liquid equilibrium behavior of dual component fuel on vapor distribution region of each component. Furthermore, the vapor distribution characteristics were investigated, simulating several crank angle conditions of a compression ignition engine.

Introduction

The spatial-temporal control of combustion processes in combustion chamber is critical to attaining better fuel economy and lower emissions in compression ignition engines. Although a number of researches including premixed charge operations have been attempted as a means of realizing this, there are still challenges associated with successful operation [1]. In response to this, the authors have pursued possibility of dual component fuels for over a decade [2]. Dual component fuels consisting of different carbon number components have anomalous physical and chemical characteristics because, for instance, (1) low boiling point (b.p.) component helps the evaporation of high b.p. one, and (2) each component separately distributes inside fuel spray due to the difference in the evaporation rate [3], causing (3) the spatial-temporal phase difference of chemical reaction due to the difference in the reactivity of each component. The present study focuses its attention on these characteristics, as shown in Fig.1. That is, this approach intends to optimize combustion processes by controlling spatial-temporal distribution of two components which have different reactivity each other. A similar approach which aimed to stratify dual-fuel according to dual-injection system including port and direct injection equipments is found in the research on premixed charge compression ignition combustion [4]. In contrast, the most important features of the authors' approach is to stratify dual-fuel by only one direct injection system, and to actively control the vapor distribution of each component .

As a first step, the present paper studies the feasibility of this approach using dual component fuel. The investigations were conducted by use of multicomponent spray model developed by the authors [5]. Firstly, by using four dual component fuels exhibiting a range of volatility, comparisons of predicted and measured spray tip penetration and liquid phase penetration were made to ensure the accuracy of this model. Also, the difference in the vapor distribution regions of two components was investigated for those fuels. Subsequently, the effects of ambient density and temperature on the vapor distribution characteristics were examined in order to explore the optimized injection timing in a compression ignition engine.

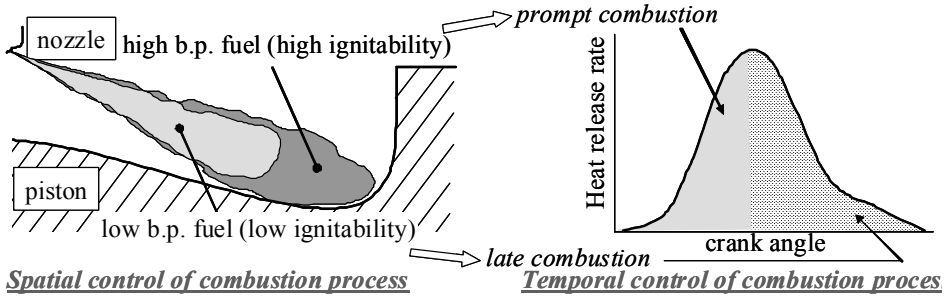

Fig.1 Spatial-temporal combustion control concept using dual component fuel

*Corresponding author, yos-wada@neptune.kanazawa-it.ac.jp

Multicomponent Spray Model

In the original versions of representative simulation codes for engine spray combustion such as KIVA, FIRE and STAR-CD, a single component fuels could be applied. Therefore, these codes never assess the properties of fuels which are commercialized in a real world. With respect to a multicomponent fuel spray, Lippert and Reitz proposed a simple evaporation model, where the fuel components were simulated by the molecular weight distribution [6]. In a model of Abraham et al. [7], the number of spray droplets was classified into the number of fuel species but each droplet consists of only one component. The authors also have reported modeling and measurements of multicomponent fuels, particularly by focusing on the distillation characteristics [8-9]. Since multicomponent fuels yield two-phase region, where liquid and vapor phases of both components are mixed at a certain molar fraction, on pressure-temperature diagram due to the molecular interaction, the evaporation of higher boiling point fuel could be promoted if fuel pressure exists in the two-phase region. Thus, the assessment of the two-phase region and vapor-liquid equilibrium would be required in order to correctly simulate the evaporation process of multicomponent spray.

The authors have developed a novel simulation model for multicomponent fuel sprays [5]. In the original version of KIVA3V [10], fuel properties are given for droplet temperature without taking into account the effect of pressure. Constant liquid density is also hypothesized regardless of a change in temperature. Therefore, to allow multicomponent fuel spray simulation and to estimate the non-ideal fuel properties, the authors' model adds the source code of NIST Mixture Property Database (SUPERTRAPP), which is capable of estimating the liquid-vapor equilibrium and the properties of mixture with twenty components, to KIVA3Vcode. The temperature and molar fraction in multicomponent liquid droplets are varied due to the evaporation of each component from droplets surface. Thus, the fuel properties in all parcels are renewed at each time step. The further information on this model is shown in the previous paper [5, 11], except for droplet breakup model. While in the authors' original model, droplets breakup had been described by TAB (Taylor Analogy Breakup) model [12], the present model employed KH-RT (Kelvin Helmholtz - Rayleigh-Taylor) model [13] in order to adequately predict liquid length. As constans of KH-RT model, B_0 and an empirical determined B_1 were set to 0.61 and 7.0, respectively. Although the latter constant should be adjusted for each fuel, the task is delegated to the other work where the effects of the conditions in the flow at the nozzle orifice and the cavitation are taken into account [14]. The liquid fuel injection was simulated using the blob injection model [15] where droplets were injected with a diameter equal to the nozzle hole diameter.

Calculation Conditions

The calculations were carried out on a 0.5-degree sector at constant. X-Z plane was composed of 30 x 50 cells for a domain of 30mm x 100mm, where 100mm was height. The fuels examined and their pressure-temperature diagram are shown in Fig.2. To understand the effect of the volatility of fuels mixed, three kinds of alkane, namely, i-pentane (iC5), i-octane (iC8) and heptamethylnonane (iC16) were mixed with n-tridecane (C13) while maintaining their mass fractions constant by 0.69. Although, in an experiment, iC16 was used for some reason [16], n-hexadecane (C16) was used instead of iC16 in the computations because there is no iC16 data in the NIST library. Fuels were supplied into air composed of nitrogen, carbon dioxide and water, from a single hole nozzle which has a diameter of 0.20mm. The injection velocity was given by assuming orifice pressure drop (Δp_{inj}) of 70MPa.

In this paper, firstly, the predicted results were validated by compared with the measured ones at ambient temperature (T_{amb}) of 800K and ambient pressure (p_{amb}) of 3.6MPa. Listed in Table1 are calculation conditions

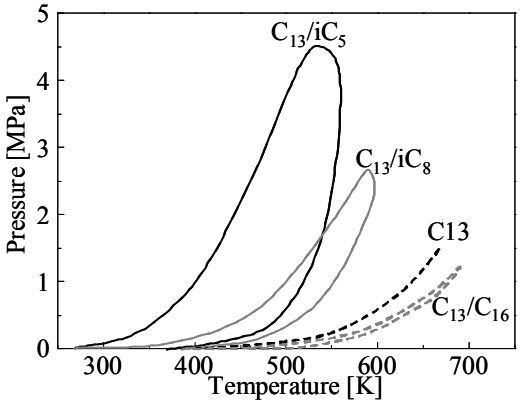

Fig.2 Pressure-temperature diagram of fuels tested

Table 1 Base calculation condition

Ambient temp., T_{amb}	[K]	800*
Ambient pressure, p_{amb}	[MPa]	3.6*
Ambient density, ρ_{amb}	[kg/m^3]	15.6*
Initial fuel temp.	[K]	300
Orifice pressure drop, Δp_{inj}	[MPa]	70
Injection quantity	[mg]	20
Nozzle diameter	[mm]	0.20

* These ambient conditions are used for model validation

equivalent to experimental ones. Subsequently, to know the effect of injection timings on vapor distribution of each component in an engine cycle, a wide variety of crank angle conditions were simulated by changing T_{amb} and p_{amb} which are given based on the measured data.

Results and Discussion

Model Validation

Comparisons of predicted and measured liquid phase penetration and spray tip penetration are made. In the experiment, spray images were taken by shadowgraph photography so that the spray tip penetration was identified as the vapor boundary of penetrating jet. The measured liquid phase penetration was also determined through image analysis and was defined as the maximum axial distance in the spray where the light transmittance was below a threshold equal to 5%. The criteria for determination of predicted liquid phase penetration was the 95% accumulated liquid mass distance from nozzle outlet [17]. Shown in Fig.3 are the measured and predicted spray tip penetrations, and liquid phase penetrations, of C13 and the dual component fuels. The physical properties of each pure component are also shown in this figure. The experimental data of the spray tip penetration was limited to 68mm because the experiments were conducted through a constant volume vessel in which the distance from nozzle tip to the lower wall is 68mm. The experimental results show that all the spray tip penetrations trace a similar trajectory each other, regardless of the fuels. Whereas, the predicted ones underestimate the spray tip penetration of lower b.p. fuel, especially in C13/iC5 and C13/iC8 dual component fuels, implying that the predicted spray tip penetration seems to be sensitive to the spray momentum depending on the kind of fuels than the experimentally-observed one. However, the multicomponent spray model does predict the difference of liquid phase penetration among the fuels correctly, indicating the good accuracy of vapor-liquid equilibrium calculation in the present model.

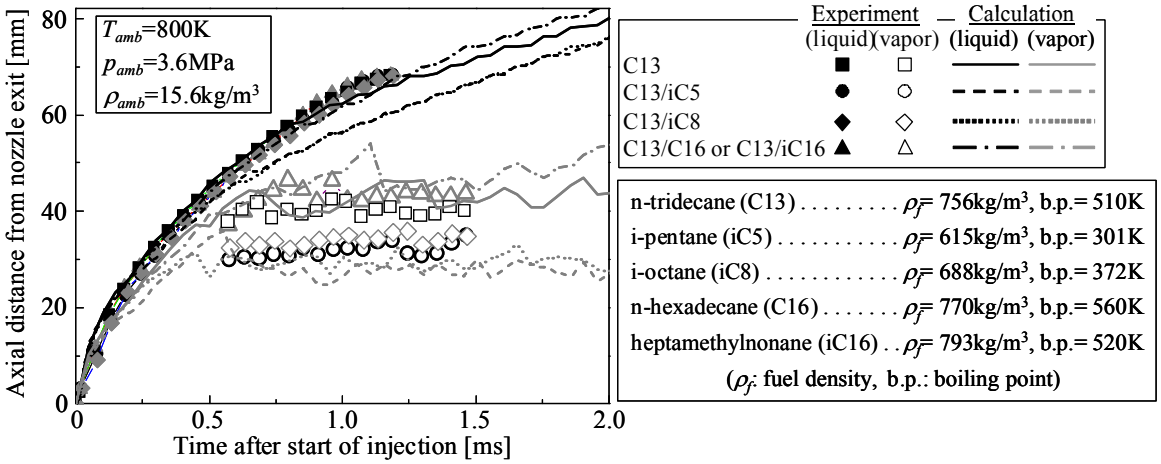

Fig.3 Comparisons of predicted and measured spray tip penetration and liquid phase penetration

Spray Characteristics of Dual Component Fuel

Based on the predicted results validated above, the spray characteristics of dual component fuel are studied. Figure 4 shows the predicted distributions of droplets size, molar fraction in the droplets and vapor concentration of each component. To ignore the difference of temporal changes in predicted spray tip penetration, all the images are selected as the data in which the spray reaches 68 mm from nozzle exit. The sprays of C13/iC5 and C13/iC8 promptly completed the evaporation compared to those of C13 and C13/C16. Paying attention to the molar fractions of the droplets, there are high concentrations of C13 molecule at the tip of liquid length in the cases of C13/iC5 and C13/C16. However, the droplets of C13/iC5 and C13/iC8 completely disappeared earlier than those of the other fuels because the evaporation of C13 upstream of the spray was enhanced by low b.p. fuel. This fact is also demonstrated in Fig.5 where the evaporation ratio of each component is compared between pure C13 and C13/iC5. The evaporation ratio, Q_{evap}/Q_{inj}, is determined as the proportion of evaporated mass quantity to injected one. It is interesting to note the difference of Q_{evap}/Q_{inj} between C13 of C13/iC5 and that of pure C13, because it is apparent that mixing iC5 promotes the evaporation of C13. This is due to the formation of two-phase region.

As mentioned in the introduction, the present approach focuses on the spatial separation of each component in the spray. Thus, the vapor concentration distribution on the spray axis is examined in Fig.6. In this figure, the vertical axis is expressed as the values normalized by the maximum vapor concentration. The C13-vapors of C13/iC5

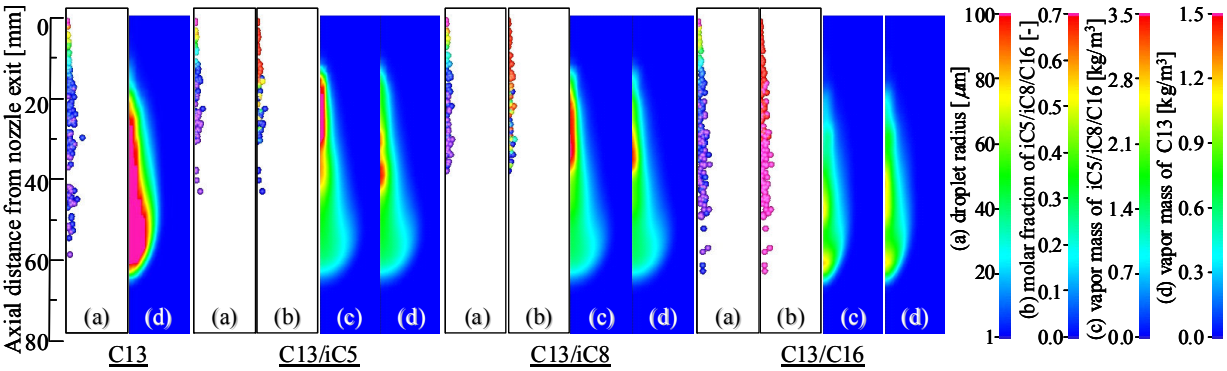

Fig.4 Predicted distributions of droplet size, molar fraction in droplets and vapor of each component (spray tip penetration ≅ 68mm, T_{amb}=800K, p_{amb}=3.6MPa)

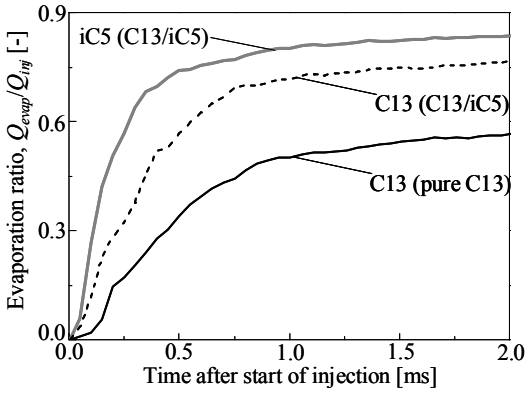

Fig.5 Comparison of evaporation rate of each component between C13/iC5 and pure C13 (T_{amb}=800K, p_{amb}=3.6MPa)

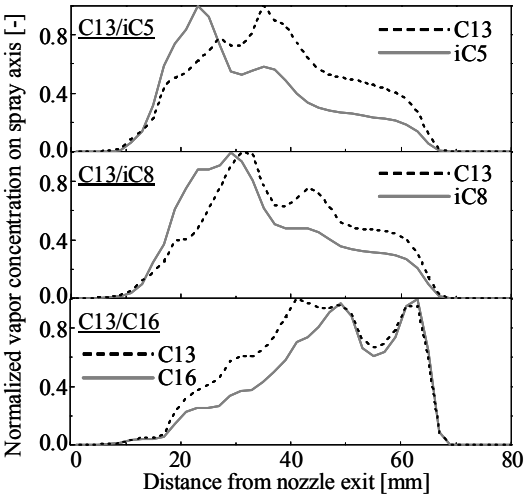

Fig.6 Normalized vapor distributions on spray axis (T_{amb}=800K, p_{amb}=3.6MPa)

and C13/iC8 starts forming closer to the nozzle than those of C13/C16. This is because the evaporation of C13 is promoted by the lower b.p. component. In addition, it is found that in the case of C13/iC5, the highest iC5-vapor concentration region is located closer to the nozzle while the C13-vapor is given as the relatively-flat distribution in the whole of the spray. Kawano et al. [3] experimentally confirmed the similar tendency with respect to multicomponent vapor distribution, using a dual component fuel composed of n-tridecane and n-pentane, although the conditions are different from the present ones. The similar trend is observed in the predicted result of C13/iC8 although the difference is smaller than that of C13/iC5. In contrast, for the C13/C16 case, there is no significant difference in the high vapor distribution regions between C13 and C16, which are ahead of the spray. Consequently, it is clear that the greater difference in volatility between two components provide the clear difference in vapor distribution regions of each component.

Effect of Injection Timing on Vapor Distribution of Each Component

As demonstrated above, there is the remarkable difference in the vapor distribution regions between the components, especially in the case of C13/iC5. Subsequently, to explore the effects of injection timing on vapor distribution, a wide range of in-cylinder pressure and temperature are given as ambient conditions in this sub-section. The ambient conditions simulated are listed in Table 2.

Figure 7 shows the changes in the predicted distributions of droplet size, molar fraction in the droplets and vapor concentration of each component with a variety of injection timings ranging, θ_{inj}, from TDC to 35 degree BTDC. Similar to Fig.4, to ignore the difference in temporal change of spray tip penetration, all the images are selected as the data in which the spray reaches 78 mm from nozzle exit. In addition, both the images of C13/iC5 and C13/iC8 are shown for comparison. The advanced injection timings slow down the evaporation rate, leading to the decrease

Table 2 Ambient conditions simulated

compression ratio [-]	14				
crank angles [degree BTDC]	TDC	15	24	35	41
Ambient temp., T_{amb} [K]	900	828	756	665	623
Ambient pressure, p_{amb} [MPa]	3.60	2.60	1.78	1.10	0.84
Ambient density, ρ_{amb} [kg/m^3]	13.9	10.9	8.20	5.74	4.68

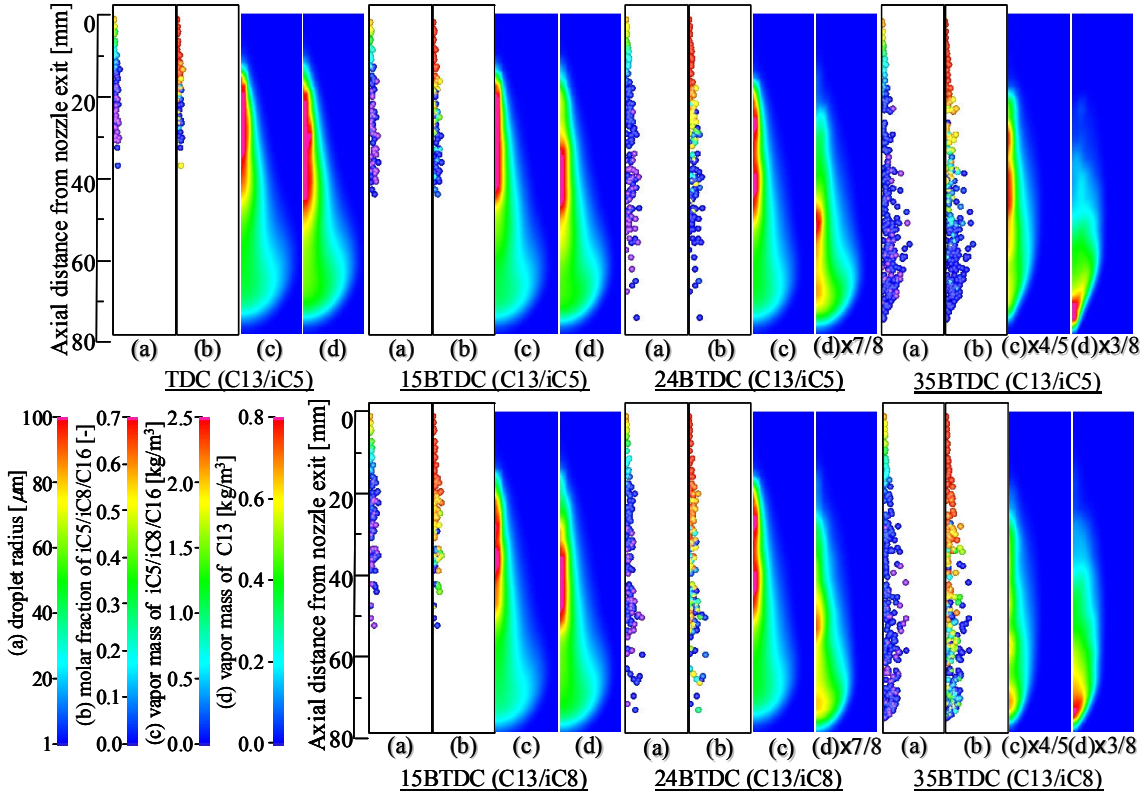

Fig.7 Predicted distributions of droplet size, molar fraction in droplets and vapor of each component for each injection timing, θ_{inj}, (spray tip penetration ≅ 78 mm, upper: C13/iC5, lower: C13/iC8)

in the vapor concentration and to the increase in the liquid phase penetration. Paying attention to the vapor distribution of C13/iC5, with advancing injection timings, the high C13-vapor concentration region drastically moves downstream of the spray but the peak of iC5-vapor concentration moderately changes the location. The similar tendency is also observed for C13/iC8. However, there is the apparent difference of molar fraction in the droplets between both fuels. At the leading portion of liquid phase, iC5-component completely evaporates while C13/iC8 droplets still contain iC8-component. This is due to the difference in volatility of dual components.

Furthermore, the distance of vapor phase centroid between higher b.p. component and lower one, L_{cent}, is analyzed to access the degree of separation between dual components vapor quantitatively. The centroid for each component is given by

$$G = \sum_{i=1}^{m}\sum_{j=1}^{n} M(x_i, z_j)\cdot L_{noz}(z_j) \Big/ \sum_{i=1}^{m}\sum_{j=1}^{n} M(x_i, z_j) \quad . \quad (1)$$

where M is the vapor mass concentration of each component, x is the coordinate in radial direction, z is the coordinate in axial direction and L_{noz} is the axial distance from nozzle exit. Thus, L_{cent} is estimated by subtracting the centroid of higher b.p. component, G_{hbp}, from that of lower one, G_{lbp}. The results of L_{cent} for C13/iC5 and C13/iC8 are presented in Fig.8 as a function of spray tip penetration. The appearance of the difference in the vapor mass centroid moves downstream by advancing the injection timings, due to the delayed start of active evaporation. However, once the L_{cent} exceeds 0 mm, the earlier the injection timings, the greater the L_{cent} is. In addition, by comparing

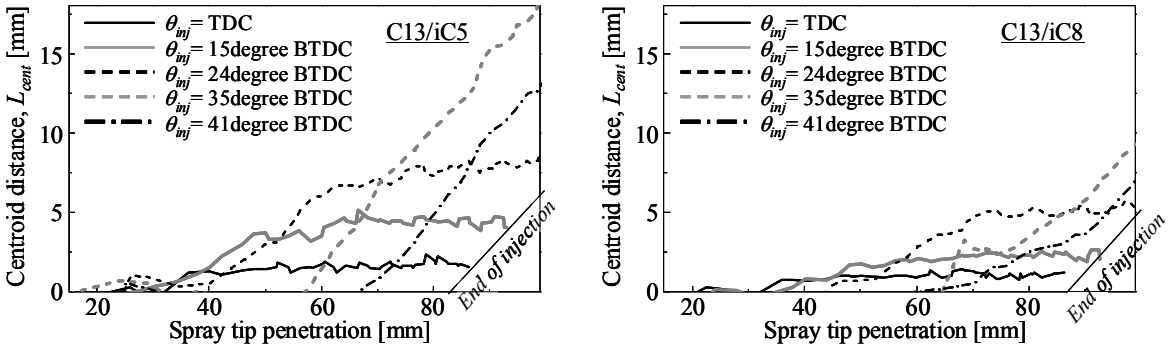

Fig.8 Distance of vapor phase centroid between dual components, L_{cent}, as a function of spray tip penetration

between the fuels tested, C13/iC5 yields greater L_{cent} compared to C13/iC8 at the region closer to nozzle. This is because the b.p. of iC8-component is not low enough and C13/iC8 droplets contain iC8-component even at the leading portion of liquid phase as described above. In summary, the spatial separation would become pronounced even in a limited geometry of combustion chamber if a dual component fuel were applied to premixed charge combustion which employs early injection timings and the volatility of lower b.p. component were high enough against the ambient condition.

Conclusion

A spatial-temporal combustion control method using a dual component fuel has been proposed in the present paper. To study the feasibility of this concept, multicomponent spray model has been applied. The results are summarized as follows:

(1) The multicomponent spray model does correctly predict liquid phase penetrations of dual component fuels which consists a wide range of boiling point components.
(2) There is the difference in vapor distribution regions of two components which are contained in a dual component fuel if the difference in boiling point between them is significant.
(3) In addition to (2), this spatial separation of vapor distribution regions is pronounced if a dual component fuel were applied to early injection timing and the volatility of lower b.p. component were high enough.
(4) The present concept has potential to spatially-temporally control the combustion processes in premixed charge compression ignition engines.

Acknowledgement

This study was supported by Grant-in-Aid for Scientific Research (Start-up) No.20860075 from the Japan Society for the Promotion of Science.

References

1. Aroonsrisopon, T., Werner, P., Waldman, J. O., Sohm, V., Foster, D. E., Morikawa, T. and Iida, M., *SAE Paper* 2004-01-1756 (2004).
2. Senda, J., Kawano, D., Hotta, I., Kawakami, K. and Fujimoto, H., *SAE Paper* 2000-01-1258 (2000).
3. Kawano, D., Senda, J., Shimada, A. and Fujimoto, H., *SAE Paper* 2002-01-0220 (2002).
4. Inagaki, K., Fuyuto, T., Nishikawa, K., Nakakita, K. and Sakata, I., *SAE Paper* 2006-01-0028 (2006).
5. Kawano, D., Senda, J., Wada, Y., Fujimoto, H., Goto, Y., Odaka, M., Ishii, H. and Suzuki, H., *SAE Paper* 2003-01-1838 (2003).
6. Lippert, A. M. and Reitz, R. D., *SAE Paper* 972882 (1997).
7. Abraham, J. and Magi, V., *SAE Paper* 980511 (1998).
8. Senda, J., Higaki, T., Sagane, Y., Fujimoto, H., Takagi, Y. and Adachi, M., *SAE Paper* 2000-01-0280 (2000).
9. Senda, J. and Fujimoto, H., *SAE Paper* 2001-01-1071 (2001).
10. Amsden, A. A., "A Block-Structured KIVA Program for Engines with Vertical or Canted Valves", Los Alamos National Laboratory Report No. LA-13608-MS.
11. Senda, J., Kawano, D., Wada, Y. and Fujimoto, H., *10th International Conference on Liquid Atomization and Spray Systems* (2003).
12. O'Rouke, P. J. and Amsden, A. A., *SAE Paper* 872089 (1987).
13. Ricart, L. M., Xin, J., Bower, G. R. and Reitz, R. D., *SAE Paper* 971571 (1997).
14. Wada, Y. and Senda, J., *10th International Conference on Liquid Atomization and Spray Systems*, Kyoto, No. B4-05-106 (2006).
15. Reitz, R. D. and Diwakar, R., *SAE Paper* 870598 (1987).
16. Wada, Y., Kitta, Y., Yamaguchi, Y., Nishimura, Y., Senda, J. and Fujimoto, H., *SAE Paper* 2006-01-3383 (2006).
17. Engine Research Center, The University of Wisconsin – Madison, http://homepages.cae.wisc.edu/~hessel/research/faq/index_faq.htm